Acceptance Simulation

Nicolás Sánchez

October 16, 2025

1 Introduction

In this document, a brief overview of the acceptance of the setup will be provided. How can we perform the simulation? To make a simple test, we can use a Monte Carlo approach to estimate the number of accepted events. This can be done by following the steps below.

- Parametrize the detector. It will be made of 2 20x20 cm^2 planes, tilted 45 degrees with respect to the beam, one located at $z = -2.5$ and the other at $z = 2.5$ cm (in the detector reference frame).
- We will generate the fission fragments in the target, that will be a 3D object with 4 cm radius and a thickness that will depend on the material (Uranium or Cerium dioxide).
- The fission fragments will be generated isotropically in the target volume.
- The fission fragments will be generated with a determined energy distribution, given by GEF simulation in the case of Uranium and, for Cerium fragments, computed with the Coulomb repulsion between 2 spheroids of charges Z_1 and Z_2 with deformation β_1 and β_2.
- Then, we will compute the trajectory of the fission fragments in the detector, taking into account the energy loss in the target, backing, gas and detector materials. The backing will only affect the fragment emitted forward.
- Finally, we will compute the acceptance of the detector, which will be defined as the fraction of fission fragments that intersect within the detector planes.

2 Simulation of Cerium fission fragments

The simulation of the Cerium fission fragments will be done distinguishing between 2 cases:

- The fission is symmetric, which means that the two fragments have almost the same mass and charge. In this case, it is easy to compute the mass and charge of the fragments, since we only have to generate a random number from a gaussian distribution, i.e. $Z_1 \sim \mathcal{N}(\frac{Z_{CN}}{2}, 4)$. In this case, the energy of the other fragment can be computed by $Z_2 = Z_{CN} - Z_1$. For the masses, we will use the UCD condition, which states that the mass-charge ratio of the compound nucleus is equal to the mass-charge ratio of the fragments, i.e. $\frac{A_{CN}}{Z_{CN}} = \frac{A_1}{Z_1} = \frac{A_2}{Z_2}$. Thus, we can obtain the masses of the fragments as $A_1 = \frac{Z_1 A_{CN}}{Z_{CN}}$ and $A_2 = A_{CN} - A_1$. The energy of the fragments can be computed using the Coulomb repulsion between two spheroids, which is given by:

$$TKE(Z_1, Z_2, A_1, A_2) = \frac{1.44 Z_1 Z_2}{R}; \tag{1}$$

where [1]

$$R = 1.2(A_1^{1/3}(1 + \frac{2}{3}\beta) + A_2^{1/3}(1 + \frac{2}{3}\beta) + d); \tag{2}$$

being β the deformation, which we will take as 0.6 [2],and d the distance between the two fragments (usually of the order of 1 fm).

- The fission is asymmetric, which means that the two fragments tend to have different charges and masses. In this case, we will assume that the fission is driven by the $Z_1 = 34$ shell. Thus, we will generate the charge of the first fragment as $Z_1 \sim \mathcal{N}(34, 2.5)$, and the second fragment will be computed as $Z_2 = Z_{CN} - Z_1$. The masses will be computed using the UCD condition as in the symmetric case. The energy of the fragments can be computed using the same formula as in the symmetric case.

How do we compute the β and d parameters? Here, we are going to use the Viola systematics, which tells us that the energy released in the fission process can be written as

$$\text{TKE} = 0.1189 \frac{Z^2}{A^{1/3}} + 7.3 \quad \text{(MeV)}. \tag{3}$$

This formula gives us the total kinetic energy of the fragments, which we can use to compute the energy of each fragment

$$KE_{HFF} = \frac{\text{TKE}}{1 + \frac{A_{HFF}}{A_{LFF}}} \tag{4}$$

$$KE_{LFF} = \frac{\text{TKE}}{1 + \frac{A_{LFF}}{A_{HFF}}} \tag{5}$$

[1] the 1.44 is a change of units to compute the TKE in eV, so the formula is basically a coulomb repulsion between the fragments, which is the cause of the acceleration of the fragments.

[2] Why are we taking this parameter as a constant? Because fixing the neck distance or the deformation does not affect the result since they are correlated, so we can fix one while varying the other, and the result should remain basically unchanged.

where HFF and LFF stand for Heavy Fission Fragment and Light Fission Fragment respectively. Then, we can compute the parameters β and d by adjusting the TKE formula given above (for $Z_1 = Z_2 = Z_{CN}/2$ and $A_1 = A_2 = A_{CN}/2$) to the result expected by the Viola systematics. We will fix d with this approach. Regarding β, we will take a constant value of 0.6, which is a reasonable value for the deformation of the fragments at scission (and, as mentioned earlier, this value is connected with d so fixing one automatically fixes the other). Note also here that we did not take into account the neutron evaporation, which will affect the mass of the fragments but not their charge. This is a detail that can be improved in the future.

3 Simulation of Uranium fission fragments

The simulation of the Uranium fission fragments will be done using the GEF code, which provides us with the masses (after neutron evaporation), charge and energy distributions of the fission fragments. We will make the simulation using 2 different neutron energies: 5 MeV, where asymmetric fission is expected to be favoured, and 100 MeV, where the symmetric channel dominates. With this approach, we will be able to compare the acceptance of the setup for different fission fragment distributions, energy losses and also to parametrize the number of events expected per angle of emission.

4 Results

All energy losses were computed using CATIMA, which is a code that computes the energy loss of ions in different materials using SRIM tables (as LISE++) [1] for energies below 10 MeV/u. The materials used in the simulation were:

- Target: UO_2 or CeO_2, with thickesses of 0.3 and 1.2 mg/cm^2, respectively.
- Backing: Al, 2.5 μm.
- Gas: C3F8, 4 mbar, 3.2 mm between anode and cathodes and 2.5 cm between target and detectors.
- Detector: 3 windows of Mylar, 0.5 mg/cm^2 each. The size of the detector was 20x20 cm^2.
- The distance between the target and the first detector was 2.5 cm, and the distance between the two detectors was 5 cm. The distance between anode and cathode was 3.2 mm and the distance traversed in target depends on the fission point.
- The distance traveled depends on the angle of emission, so the energy loss will also depend on this angle, and in each step we will compute the time taken to traverse it in order to obtain the distribution of time differences between both anodes.

4.1 Cerium fission fragments

Symmetric fission

We will begin by showing the charge distribution of the accepted fragments, which is shown in figure 1. As expected, the distribution is centred around $Z = 29$.

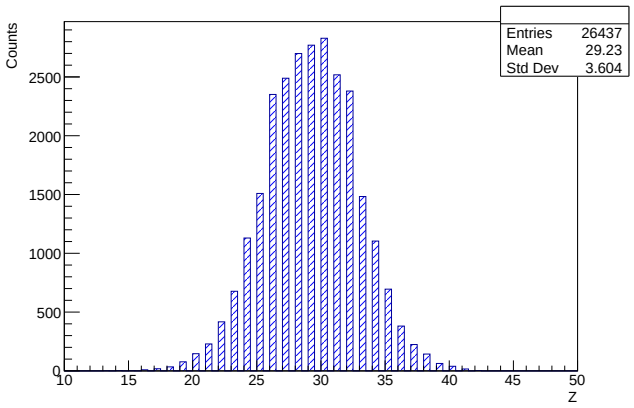

Figure 1: Charge distribution of the fragments for symmetric fission of Cerium.

The energy distribution of the fragments is shown in figures 2 and 3. The binning is quite coarse since there are only a few possible initial energies.

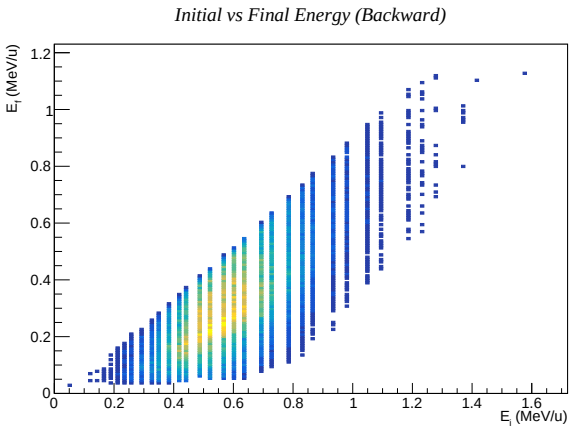

Figure 2: Energy distribution of the backward-emitted fragments for symmetric fission of Cerium.

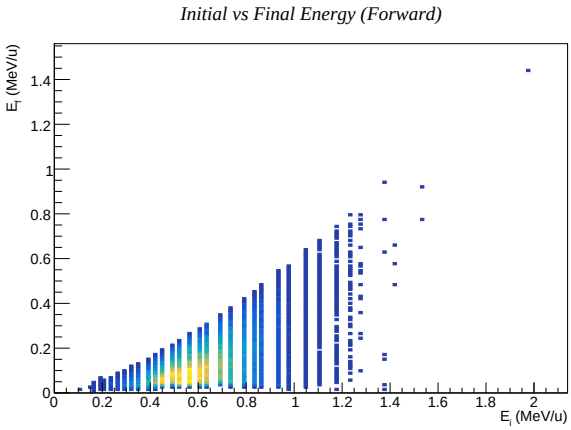

Figure 3: Energy distribution of the forward-emitted fragments for symmetric fission of Cerium.

Another aspect worth studying is the contribution to the energy loss of each material. This can be done for the backward and forward emitted fragments, being the main difference that the forward one has a backing contribution, in addition to the target and gas contributions. The results are shown in figures 4 and 5.

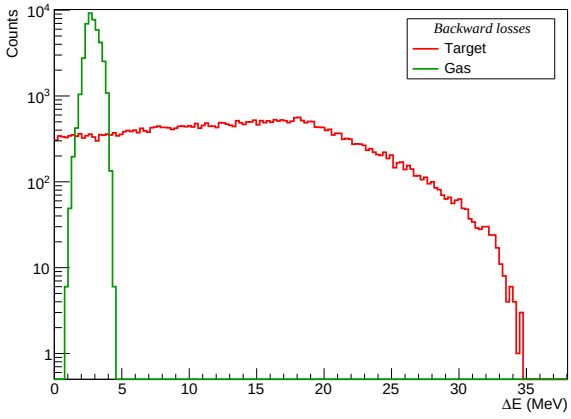

Figure 4: Energy loss contribution of each material for the backward-emitted fragments for symmetric fission of Cerium.

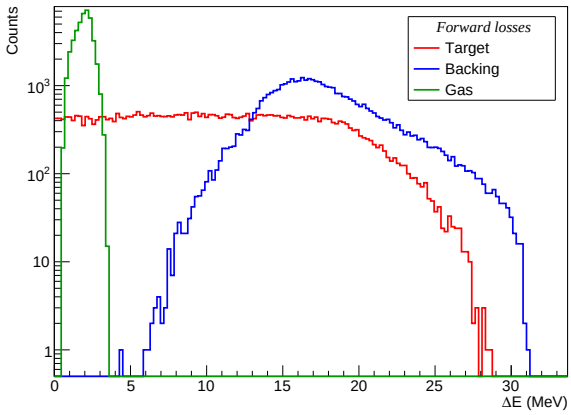

Figure 5: Energy loss contribution of each material for the forward-emitted fragments for symmetric fission of Cerium.

Once we have the energy distribution, we can see the position distribution of the impact points in the detectors. In order to analyze the results, we have to take into account two possible reference frames: the detector frame (local), and the beam reference frame (global). Thus, the results are attached in the figures below.

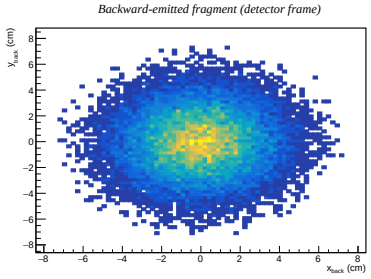

(a) Backward-emitted fragments in detector frame.

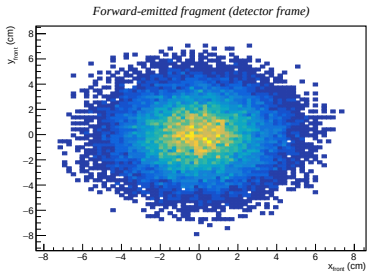

(b) Forward-emitted fragments in detector frame.

Figure 6: Position distribution of the impact points in the detectors for symmetric fission of Cerium in the detector frame.

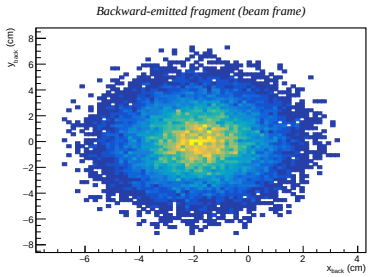

(a) Backward-emitted fragments in global frame.

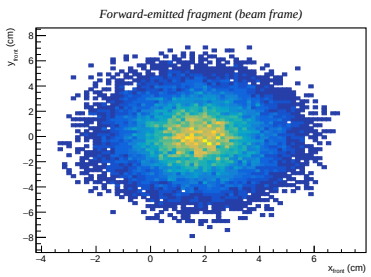

(b) Forward-emitted fragments in global frame.

Figure 7: Position distribution of the impact points in the detectors for symmetric fission of Cerium in the global frame.

What we can see from figures 6 and 7 is that, in the beam frame, the X-coordinate range is modified, since in this reference system the detector does not lie in a constant Z plane. In addition, in the beam frame we can see that the emission is not in the center of the detector, since the distribution is centered around (0,2) and (0,-2) cm for the forward and backward detectors respectively. Another interesting aspect to study is the efficiency of detection, which is defined as the ratio between the number of accepted events (those that hit both detectors) and the total number of generated events. The results are shown in figure 8. What we can see is that the efficiency of detection is around 13 %, allowing us to reach polar angles around 100 degrees.

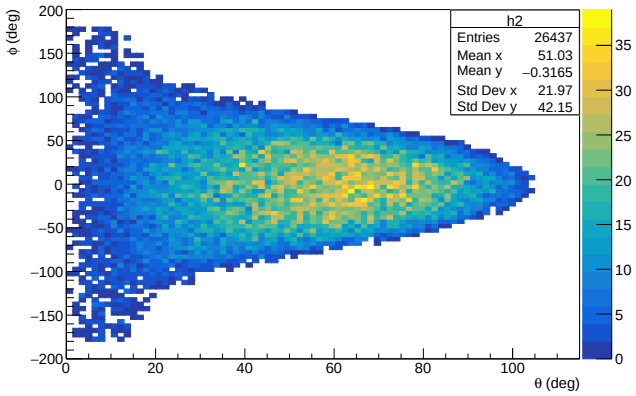

Figure 8: Efficiency of detection for symmetric fission of Cerium.

Finally, we can compute the time difference between both anodes, which is shown in figure 9. The time difference is computed as $t_1 - t_0$, so a positive value means that the forward-emitted fragment arrives later than the backward-

emitted one. We can also see a tail in the left part of the plot (negative time differences), which comes mainly from events where the backward-emitted fragment has a very low energy (heavy fission fragment) and thus takes a long time to reach the detector. This tail is not in the right part because for the forward-emitted fragments, the heavy fragments do not reach the detector in such cases because of the backing. Possible sources of uncertainty or discrepancy are the fact that in the real simulation our time difference comes from the anode signal. This signal can be triggered by electrons coming from both cathodes, each one traveling a different distance thus affecting the time difference.

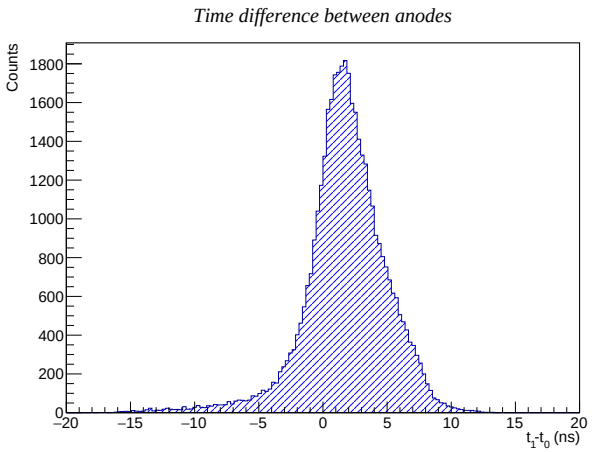

Figure 9: Time difference between both anodes for symmetric fission of Cerium.

Furthermore, we can study the time difference versus the angle of emission (in the beam frame), and versus the sum of energy deposited in the gas volume in between the anode-cathode region.

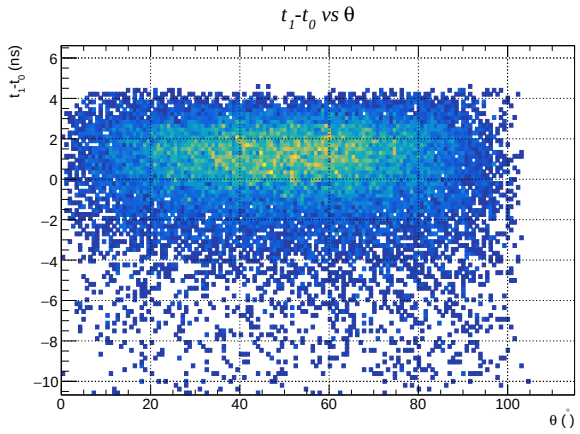

Figure 10: Time difference between both anodes versus the angle of emission for symmetric fission of Cerium.

In figure 10, we can see that the number of events is bigger in the region of $\theta \sim 45°$, which is expected because is the normal of both target and backing, thus in this emission angle the distance traversed is minimum. In addition, we can see that we cover a broad angular region, which is essentially the reason why the PPACs were tilted for this experiment. Finally, we can see the time difference versus the sum of energy deposited in the gas volume of the forward detector, which is shown in figure 11. In this case, what we can see is that the tail for negative time differences corresponds to larger depositions in the gas between cathodes and anode for the forward-located detector.

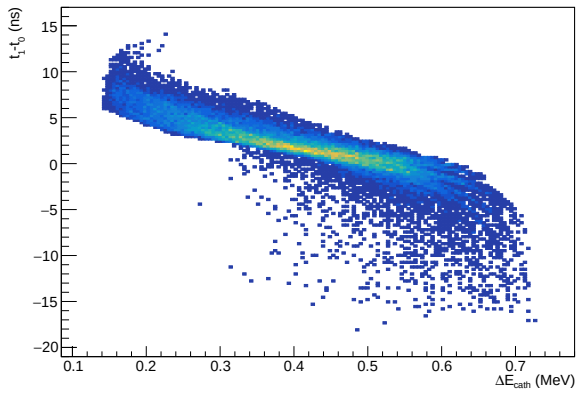

Figure 11: Time difference between both anodes versus the sum of energy deposited in the gas (forward fragment) for symmetric fission of Cerium.

In order to see where this events stem from, we can make a plot of the

time difference against the initial energy of the forward-emitted fragment, and identify the events with a negative time difference to those with the biggest initial energies (light fission fragments).

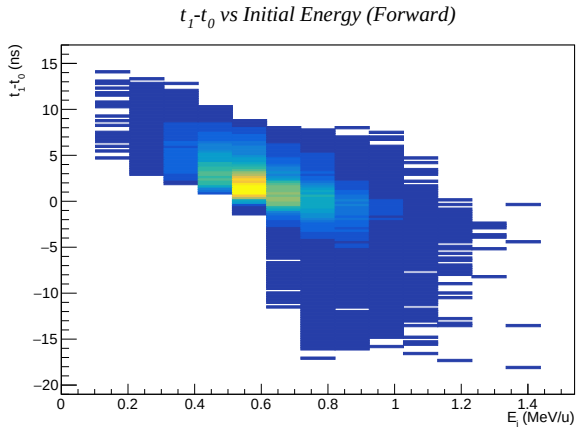

Figure 12: Time difference between both anodes versus the initial energy of the forward-emitted fragment for symmetric fission of Cerium.

Asymmetric fission

We will now show the results for the asymmetric fission of Cerium. The charge distribution of the accepted fragments is shown in figure 13.

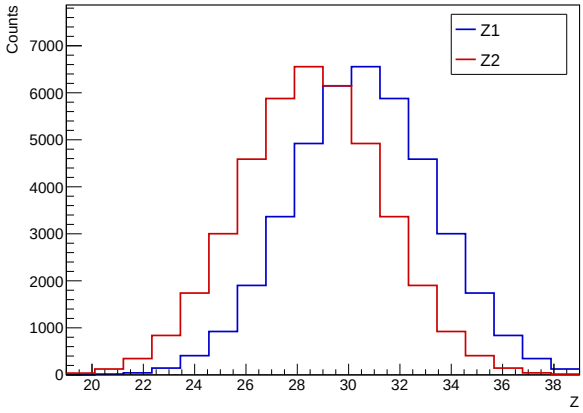

Figure 13: Charge distribution of the fragments for asymmetric fission of Cerium.

As mentioned earlier, in this case we are assuming that the fission process

is driven by the $Z = 34$ shell, but the results show a closer distribution of charge between the two fragments, which can be explained by the fact that fission events with a larger asymmetry in charge are not accepted since the heavy fragment is stopped before reaching the detector. If we now take a look at the time difference between both anodes, we can see that the distribution is also heavily affected by the acceptance, as shown in figure 14. This distribution has a broader peak than in the symmetric case.

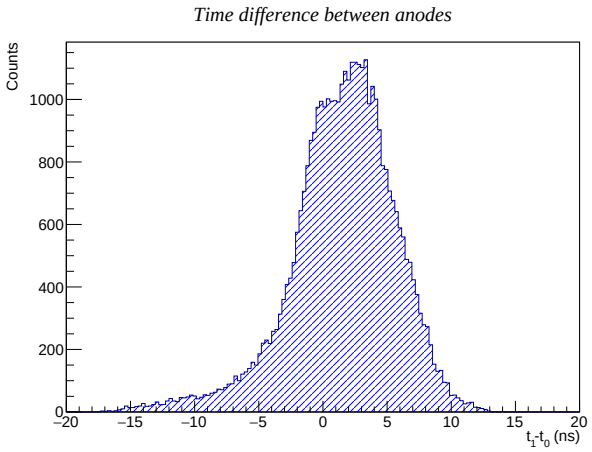

Figure 14: Time difference between both anodes for asymmetric fission of Cerium.

If we look at the time difference versus the angle of emission, we can see that the distribution is quite similar to the symmetric case, as shown in figure 15.

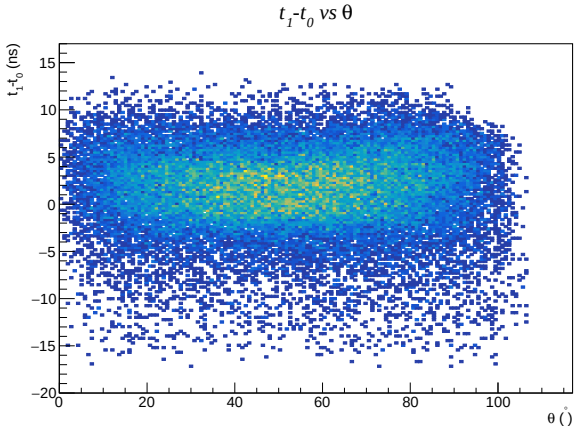

Figure 15: Time difference between both anodes versus the angle of emission for asymmetric fission of Cerium.

Finally, we can see the time difference versus the sum of energy deposited in the gas volume of the forward detector, which is shown in figure 16.

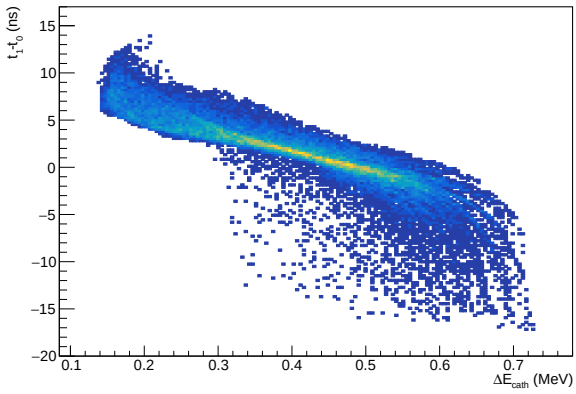

Figure 16: Time difference between both anodes versus the sum of energy deposited in the gas (forward fragment) for asymmetric fission of Cerium.

4.2 Uranium fission fragments

In this section, we will show the results for Uranium-238 fission fragments, distinguishing between two different neutron energies: 5 MeV and 100 MeV. We will make an analog study as in the previous section, showing the distribution of the most important observables.

$E_n = 5$ **MeV**

We will begin by showing the charge distribution of the accepted fragments, which is shown in figure 17.

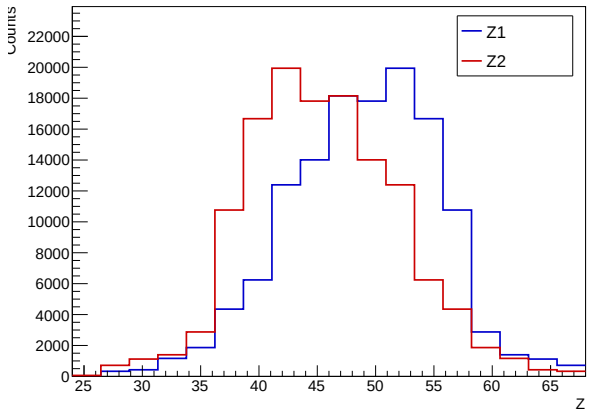

Figure 17: Charge distribution of the fragments for Uranium fission with $E_n = 5$ MeV.

As expected, the heavy fission fragment peak is around $Z = 52 - 56$. The energy distribution of the fragments is shown in figures 18 and 19. What we can see is that, for the forward-emitted fragment there is a broader distribution of final energies for a given initial energy. This again can be explained by taking into account the bigger amount of layers traversed, thus a bigger energy loss and straggling.

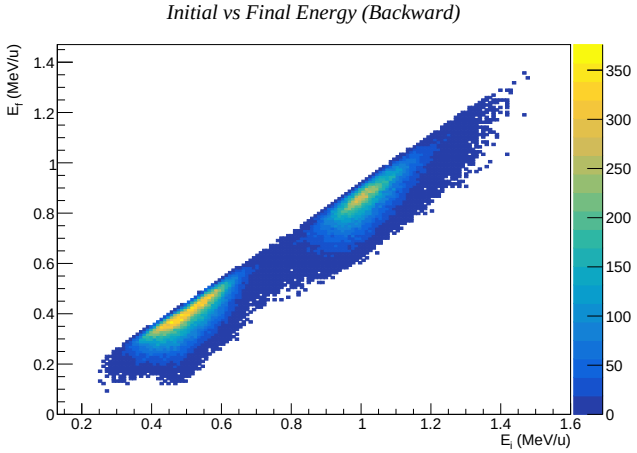

Figure 18: Energy distribution of the backward-emitted fragments for Uranium fission with $E_n = 5$ MeV.

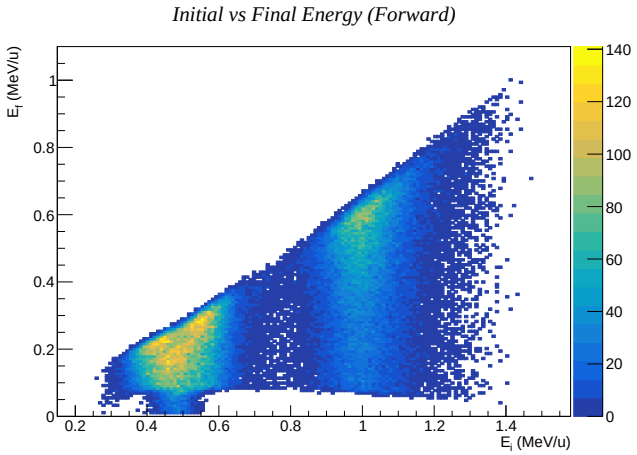

Figure 19: Energy distribution of the forward-emitted fragments for Uranium fission with $E_n = 5$ MeV.

If we study the efficiency of detection, we can see a bigger acceptance (in polar angle) than in the case of Cerium ($\theta_{max} = 100°$ for Cerium, 120 for Uranium), which is expected since the energy of the fragments is bigger. The results can be seen in figure 20.

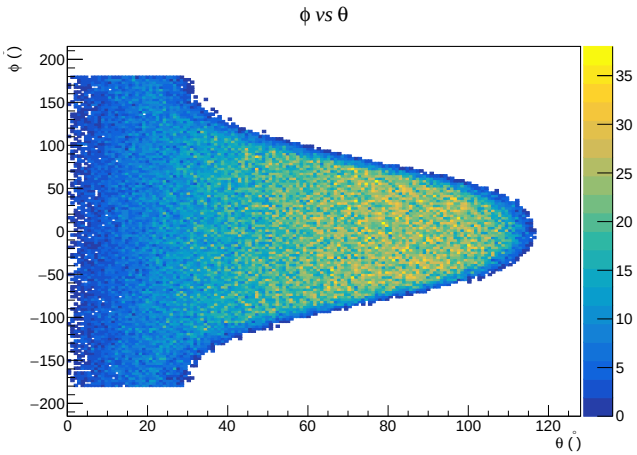

Figure 20: Efficiency of detection for Uranium fission with $E_n = 5$ MeV.

If we now take a look at the time difference between both anodes, we can see the distribution shown in figure 21. The distribution is characterised by 2 peaks. The first peak is higher and narrower, since it corresponds to the case where the light fission fragment is emitted forward, thus having a higher velocity and a smaller energy loss. This can be confirmed by plotting the time difference

against the intial energy of the forward-emitted fragment, as shown in figure 22, where we can see that the left peak corresponds only to events with a higher initial energy (light fission fragments). If we see the correlation between time difference and final energy (see fig. 23), we can see that the peak at positive time differences is more spread since it receives contributions from both light and heavy fragments, whereas as the final energy increases, we go to the left peak, where only light fragments contribute (higher final energies).

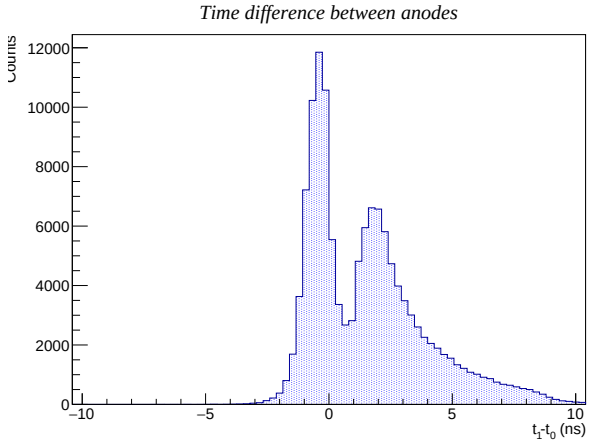

Figure 21: Time difference between both anodes for Uranium fission with $E_n = 5$ MeV.

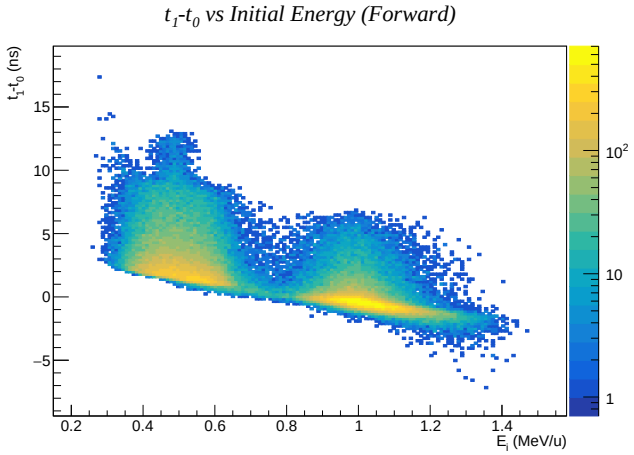

Figure 22: Time difference between both anodes versus the initial energy of the forward-emitted fragment for Uranium fission with $E_n = 5$ MeV.

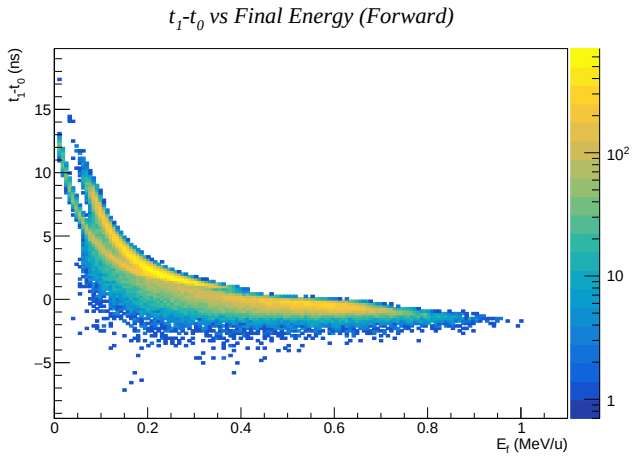

Figure 23: Time difference between both anodes versus the final energy of the forward-emitted fragment for Uranium fission with $E_n = 5$ MeV.

Now, we can continue our analysis by plotting the time difference against the angle of emission, as shown in figure 24.

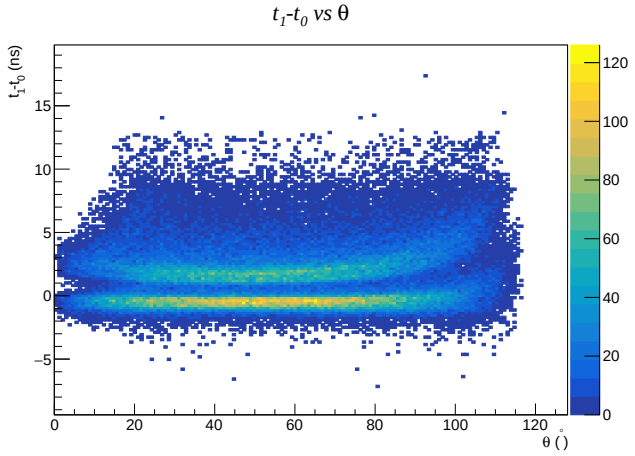

Figure 24: Time difference between both anodes versus the angle of emission for Uranium fission with $E_n = 5$ MeV.

We shall point out here that the distribution is symmetric with respect to $\theta = 45°$, which is expected since the fragments traverse less matter in this direction, and thus they will traverse the same amount of matter as they deviate the same quantity from $\theta = 45°$ to higher or lower angles. Finally, we can see the time difference versus the sum of energy deposited in the gas volume of the

forward detector, which is shown in figure 25, where we can easily distinguished between the heavy and light fragments when emitted forward. The light one is defined as the one that tends to deposit more energy in the gas, thus being the accumulation of points in the right part of the plot. The heavy fragment has a more spread distribution of times for a given energy deposition.

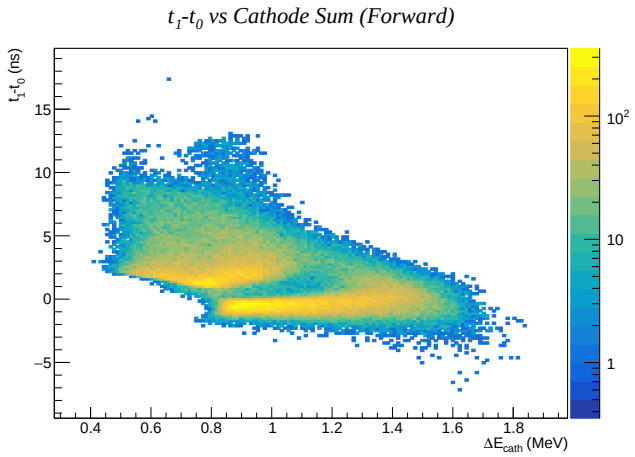

Figure 25: Time difference between both anodes versus the sum of energy deposited in the gas (forward fragment) for Uranium fission with $E_n = 5$ MeV.

$E_n = 100$ **MeV**

In this section, we will show the results for Uranium-238 fission fragments with a neutron energy of 100 MeV. We will make an analog study as in the previous section, showing the distribution of the most important observables. We will begin by showing the correlation between the initial and final energy for the forward and backward emitted fragments, which are shown in figures 26 and 27. What we can see is that the final energy is more spread for a given initial energy in the case of the forward-emitted fragment, which is expected since it traverses more matter (backing, target and gas).

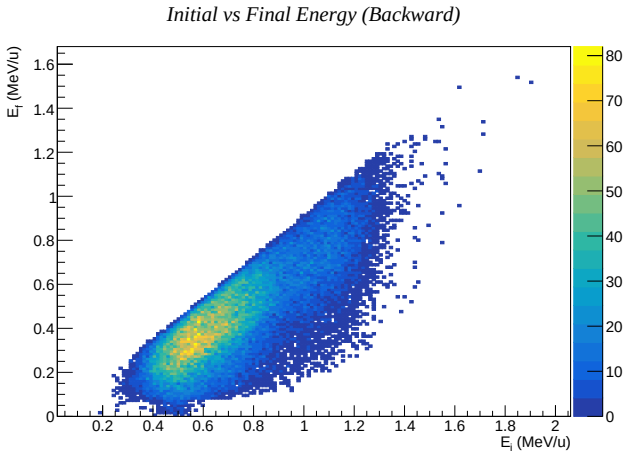

Figure 26: Energy distribution of the backward-emitted fragments for Uranium fission with $E_n = 100$ MeV.

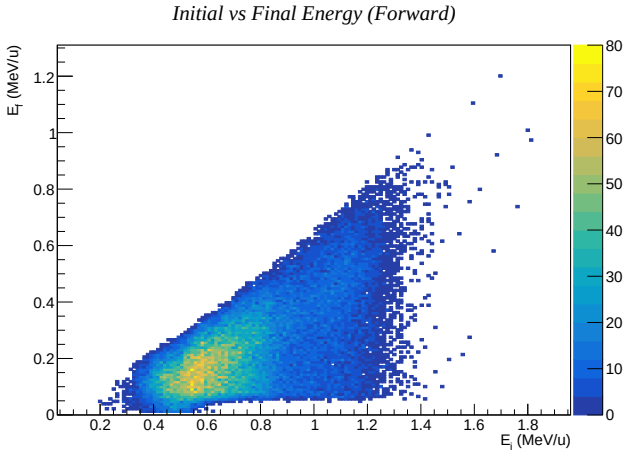

Figure 27: Energy distribution of the forward-emitted fragments for Uranium fission with $E_n = 100$ MeV.

The efficiency of detection is shown in figure 28, where we can see that the acceptance is different with respect to the 5 MeV case. First, there is an obvious effect of the statistics, because GEF gave an output of 100000 fission events at 100 MeV and 200000 events at 5 MeV. But the most striking difference is that the efficiency in the azimuthal angle begins to drop at smaller polar angles in the case of 100 MeV. Why?

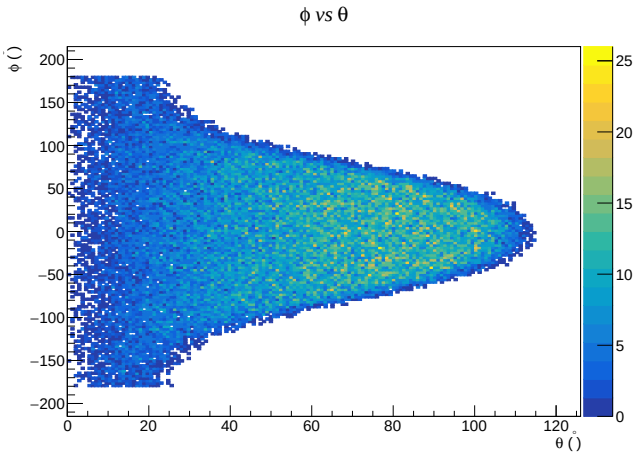

Figure 28: Efficiency of detection for Uranium fission with $E_n = 100$ MeV.

If we look at the time difference between both anodes, we can see the figure shown in figure 29. As expected, the distribution presents only one peak, since at this energy the symmetric channel dominates, thus the fragments have similar energies and masses. Note that the mean of the distribution is not zero, since the forward-emitted fragment takes a longer time to reach the anode.

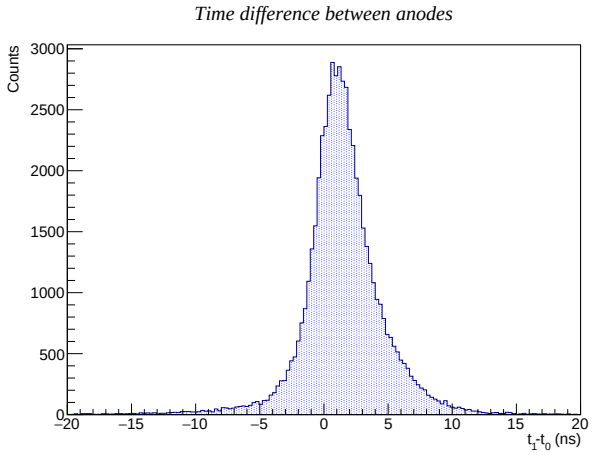

Figure 29: Time difference between both anodes for Uranium fission with $E_n = 100$ MeV.

If we see the correlation between time difference and final energy (see fig. 30), we can see that the distribution is more symmetric than in the 5 MeV case, since both fragments have similar energies and masses.

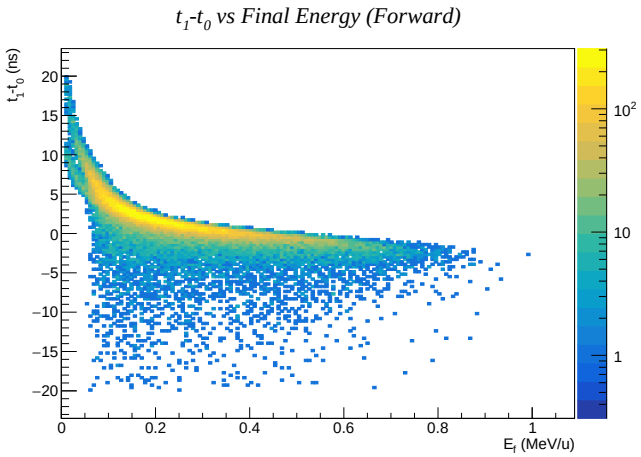

Figure 30: Time difference between both anodes versus the final energy of the forward-emitted fragment for Uranium fission with $E_n = 100$ MeV.

If we now take a look at the time difference versus the angle of emission, as shown in figure 31, we can see that the time difference gets bigger at larger angles, thus a small curvature at the right part of the plot is observed, as expected.

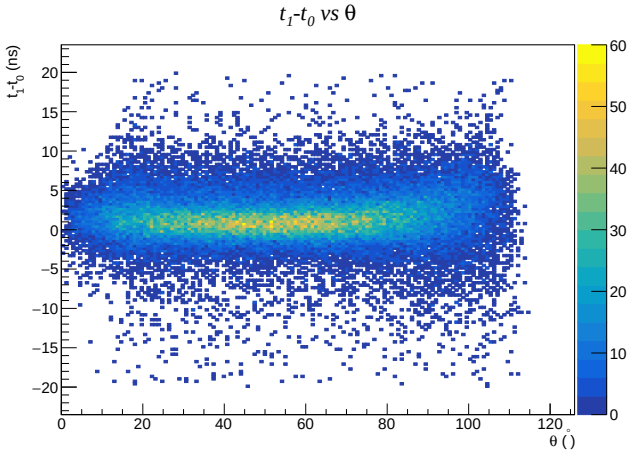

Figure 31: Time difference between both anodes versus the angle of emission for Uranium fission with $E_n = 100$ MeV.

Finally, we can see the time difference versus the sum of energy deposited in the gas volume of the forward detector, which is shown in figure 32.

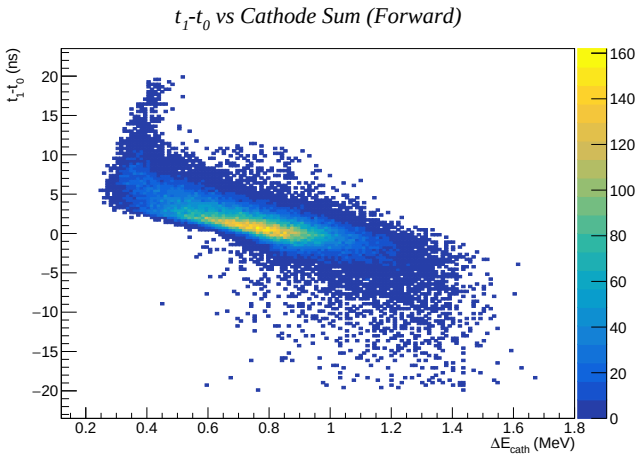

Figure 32: Time difference between both anodes versus the sum of energy deposited in the gas (forward fragment) for Uranium fission with $E_n = 100$ MeV.

References

[1] J.F. Ziegler, J.B. Biersack, U. Littmark, *The Stopping and Range of Ions in Solids*, Vol. 1, Pergamon Press (1985).